Unconventional Floquet topological phases in the Su-Schrieffer-Heeger lattice

Dunkan Martínez,[1] Yuriko Baba,[2,3] Benjamín Santos,[4] Rodrigo P. A. Lima,[5,6] Pedro Orellana,[7] Francisco Domínguez-Adame,[1] and Alexander López[1,8,9,*]

[1]*GISC, Departamento de Física de Materiales, Universidad Complutense de Madrid, Madrid, Spain*
[2]*Condensed Matter Physics Center (IFIMAC), Universidad Autónoma de Madrid, E-28049 Madrid, Spain*
[3]*Instituto de Estructura de la Materia IEM-CSIC, Serrano 123, E-28006 Madrid, Spain*
[4]*M82 Consulting Services G.P., Laval, Canada*
[5]*GISC and InterTEP, Departamento de Física, Facultad de Ciencias Ambientales y Bioquímica, Universidad de Castilla-La Mancha, E-45071 Toledo, Spain*
[6]*GFTC, Instituto de Física, Universidade Federal de Alagoas, Maceió AL 57072-970, Brazil*
[7]*Departamento de Física, Universidad Técnica Federico Santa María, Casilla 110 V, Valparaíso, Chile*
[8]*Institute for Theoretical Physics, University of Regensburg, D-93040 Regensburg, Germany*
[9]*Escuela Superior Politécnica del Litoral, ESPOL, Departamento de Física, Facultad de Ciencias Naturales y Matemáticas, Campus Gustavo Galindo Km. 30.5 Via Perimetral, P.O. Box 09-01-5863, Guayaquil, Ecuador*

(Received 1 September 2025; revised 19 November 2025; accepted 24 December 2025; published 20 February 2026)

Topological materials, known for their edge states robust against local perturbations, hold promise for next-generation quantum technologies, but remain scarce in nature and challenging to realize in static systems. The Su-Schrieffer-Heeger chain is a one-dimensional system with a well-known topological phase protected by chiral symmetry, although its static control is limited. To overcome these limitations, we propose to use high-frequency monochromatic driving and modulated amplitude pulses to induce and switch the Floquet topological phases even when the chiral symmetry is dynamically broken. Using a Kramers-Henneberger-like transformation, we encode all Floquet sidebands into a single effective Hamiltonian. We demonstrate that both monochromatic and experimental pulse protocols (Gaussian and fast-beating envelopes) can induce topological edge states, enabling dynamic phase switching. Notably, fast-beating modulations require significantly lower-field amplitudes than monochromatic ones, especially with a larger intracell dimer separation. Our findings offer an experimentally feasible route for Floquet engineering, paving the way for ultrafast and energy efficient control of topological phases in quantum platforms, opening up different possibilities in the field of dynamic quantum materials.

DOI: 10.1103/hh2x-mbrb

I. INTRODUCTION

Topological materials have received a great deal of attention since their discovery [1–6]. Their engineering via periodically driving time-dependent interactions has been shown to be a suitable means to manipulate material properties on demand. These topological materials can support a bulk band gap, but have protected gapless edge states at their boundaries. Spinless systems have been shown to possess protected edge states in the absence of time-reversal symmetry [7]. In pioneering works [8–21], it is shown that nontrivial topological properties can be induced in static systems by periodically driving fields, leading to the so-called Floquet topological insulator (FTI), which show boundary edge states that are not achievable within the static scenario. Generally speaking, the topological response of a physical system can be assessed via topological invariants, such as the Chern number, the spin-Chern number $\mathcal{Z}_2$, and higher-order extensions. The tenfold classification and its extensions allow one to determine which class belongs to a given system solely by its symmetries and spatial dimension [22–26]. An interesting model for realizing FTI phases in periodically driven lattices, valid for arbitrary driving regimes, is presented in Ref. [27], demonstrating that nonadiabaticity drives transitions between distinct topological phases.

Remarkably, several works on FTIs focus on constant-amplitude periodic interactions. However, maintaining a constant-amplitude electric field can be challenging in experimental setups, whereas the use of finite-duration pulses modulated in amplitude and frequency, achievable within current technological implementations, allows for a more realistic description of the actual experimental scenario [28]. For example, recent advances in time-dependent angle-resolved photoemission spectroscopy have enabled access to ultrafast electron states and their spin dynamics in solids [29–32]. From a theoretical point of view, the description of such experimental scenarios needs to take into account the nonperiodicity of the systems, i.e., regimes beyond conventional Floquet engineering. This can be done with direct solutions to the time-dependent problem or with hybrid formalisms, such as the so-called $t - t'$ formalism. The latter describes the effects of the driving field within the Floquet picture by using two distinct timescales, namely the timescale of the envelope amplitude and the period of the external field [28,33–36].

Although the $t - t'$ formalism brings a powerful tool for interpreting the time evolution under nonperiodic pulses within

*Contact author: alexlo08@ucm.es

the Floquet picture, it has important limitations when dealing with strongly nonadiabatic regimes. Additionally, it could be computationally expensive since several sidebands are necessary for the correct description of intense radiation fields. To overcome these limitations and in order to deal with arbitrary pulse shapes, this work uses a Kramers-Hennenberg-like transformation [37]. This transformation is less computationally expensive and allows us to obtain the zero-order renormalized sideband contribution directly.

In this work, we focus on the periodically driven one-dimensional Su-Schrieffer-Heeger (SSH) chain [38–42] where intense pulses generate nontrivial Floquet topological states protected by the chiral symmetry. We show that despite the instantaneous breaking of chiral symmetry, a dipolar periodic driving protocol can still induce robust topological edge states, even in parameter regimes where the static system remains topologically trivial. Moreover, the amplitude-modulated protocols enable the realization of these nontrivial topological phases at lower values of the light-matter coupling strength, compared to the ones required for constant-amplitude modulations. We expect these features to be advantageous for actual experimental realizations of our theoretical proposal within the realm of spectroscopic experimental implementations. We characterize these topological transitions by an invariant defined in real space and by observables such as the time-averaged density of states (DOS), that is related to the average probability of occupation of the sidebands. The structure of this work is as follows. In Sec. II the topological invariant employed is defined, and in Sec. III we apply the Kramers-Henneberger transformation to effectively solve the dynamical response of a one-dimensional SSH chain subject to a periodically driving electric field with constant amplitude, showing the time-averaged DOS tunability of the quasienergy spectrum. Then, in Sec. IV we extend the analysis to amplitude-modulated electric field configurations, comparing explicitly Gaussian and harmonic-modulated pulses, which constitute two experimentally relevant driving protocols. Section V presents the concluding remarks.

II. TOPOLOGICAL CHARACTERIZATION OF DRIVEN SYSTEMS

The topological nature of a system is characterized by the invariant associated with its symmetry class [23]. In translationally invariant systems, this quantity can be evaluated in momentum space through global invariants such as the Chern number [43] or the winding number [44]. However, for finite or disordered systems, where translational symmetry is broken, these momentum-space formulations are no longer applicable. In such cases, one must resort to real-space quantities such as local topological markers, which generalize the notion of bulk invariants to nonperiodic settings [45,46].

Since we focus on the SSH chain, which belongs to the AIII symmetry class, the relevant topological quantity is the winding number. In real-space formulations, its local counterpart, named the winding marker, can be expressed as

$$\nu(x) = -2\pi i \,\mathrm{Tr}_x(P\Gamma[X,P]), \tag{1}$$

where Tr_x denotes the trace over the spatial coordinates, $P = \sum_{E_n<E_F} |n\rangle\langle n|$ is the projector onto the occupied states, X is the position operator, and Γ is the chiral operator. However, evaluating $\nu(x)$ requires constructing the full projector P, which involves all occupied eigenstates and rapidly becomes computationally demanding for large or dense systems. To circumvent these limitations, the spectral localizer formalism has been introduced as an alternative real-space approach [47]. It encodes the same topological information by combining the Hamiltonian and position operators within a Clifford algebra framework into a single Hermitian matrix known as the spectral localizer $\mathcal{L}_{(x,E)}$. This construction is such that, when the position and Hamiltonian operators commute, the localizer is block-diagonal and its signature (i.e., the difference between the number of positive and negative eigenvalues) is zero, indicating a topologically trivial phase. In contrast, when the operators fail to commute, the localizer develops a nonzero signature, and half of this value defines the topological index of the system [48]

$$\nu = \tfrac{1}{2}\mathrm{sig}(\mathcal{L}_{(x,E)}), \tag{2}$$

where $\mathrm{sig}(\mathcal{O})$ stands for the signature of the operator $\mathcal{O}$.

For the AIII symmetry class, the localizer is defined as

$$\mathcal{L}_{(x,E)} = [\kappa(X - x\mathbb{1}) - i(H - E\mathbb{1})]\Gamma, \tag{3}$$

where x specifies the real-space position around which the topological properties are locally evaluated (usually $x = 0$ is set to be in the middle of the chain), E sets the energy reference used to probe the occupied and unoccupied subspaces ($E = 0$), and κ is a parameter that weights the Hamiltonian and the position operator. This dependence allows the spectral localizer to distinguish between regions with different local topological character, such as bulk and edge domains, or between energies inside and outside the bulk gap. When we are dealing with a periodically driven system, the Hamiltonian we need to use for defining the spectral localizer is the effective Floquet Hamiltonian [49] given by

$$H_{\mathrm{eff}} = \frac{i}{T}\log\left[\mathcal{T}\exp\left(-i\int_0^T H(t)dt\right)\right], \tag{4}$$

where T is the period of the driving $T = 2\pi/\Omega$ (or Ω_- in the periodic envelope laser pulse discussed below), and $\mathcal{T}$ is the time-ordering operator.

As the signature of the spectral localizer encodes the topological index of the system, the corresponding topological phase remains invariant as long as the localizer gap does not close. Consequently, the absolute value of the smallest eigenvalue of the localizer,

$$\mu = \min\{|\mathrm{eigenvalue}[\mathcal{L}_{(x,E)}]|\}, \tag{5}$$

provides a quantitative measure of the robustness of the topological phase. A large μ indicates that the system is far from a topological transition, whereas a vanishing μ signals the closing of the localizer gap and the onset of a possible topological phase transition.

III. PERIODICALLY DRIVEN SSH CHAIN

We consider spinless electrons in a periodically driven one-dimensional SSH chain with N dimers, with staggered hopping energies, and subject to a time-dependent uniform

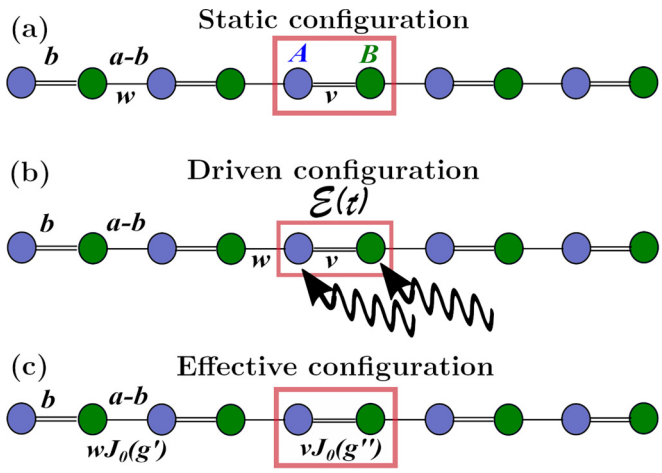

FIG. 1. Schematic representation of the (a) static, (b) driven, and (c) effective one-dimensional SSH chain. The lattice and intracell dimer separations are denoted as a and b, respectively. The unit cell is highlighted within the red rectangle. The intracell and intercell hopping energies are v and w, respectively. $\mathcal{E}(t)$ is the time-dependent electric field along the chain and the effective light-matter couplings are $g' = (1 - b/a)g$ and $g'' = gb/a$ with $g = ea\mathcal{E}_0/\hbar\Omega$. Here, $\mathcal{E}_0$ and Ω denote the amplitude and frequency of the driving field, respectively.

electric field, as shown schematically in Fig. 1. The static Hamiltonian for the bipartite system is given as [27,40]

$$H_S = v\sum_{\ell=1}^{N}|\ell\rangle\langle\ell|\sigma_x + w\sum_{\ell=1}^{N-1}|\ell+1\rangle\langle\ell|\sigma_+ + \text{H.c.}, \tag{6}$$

where $|\ell\rangle$ represents the two orbitals located in the ℓth unit cell and $\sigma_\pm = (\sigma_x \pm i\sigma_y)/2$ are the usual ladder operators, with Pauli matrices acting in the inner space of the $\{A, B\}$ sublattices. In addition, v and w denote the intra- and intercell hoping energies, respectively.

When the chain is subject to a periodic driving protocol, via a uniform monochromatic electric field directed along the chain and described within the dipolar approximation, the total time-dependent Hamiltonian $H(t) = H_S + V(t)$ reads

$$H(t) = H_S + e\mathcal{E}(t)x, \tag{7}$$

with $-e$ the electric charge of the electron, $\mathcal{E}(t)$ the time-dependent electric field, and x the position operator with respect to the center of the chain. Within this formulation, the driving interaction is symmetric with respect to the reflection operation $x \to -x$ (besides an irrelevant phase shift). In the tight-binding approach, the interaction takes the form

$$V(t) = e\mathcal{E}(t)\sum_{\ell=1}^{N}\left[\frac{(2\ell - N - 1)}{2}a\mathbb{1}_\sigma - \frac{b}{2}\sigma_z\right]|\ell\rangle\langle\ell|, \tag{8}$$

with a being the lattice spacing and b the distance between the sublattice atoms [27]. Here, $\mathbb{1}_\sigma$ is the identity operator in the degree of freedom of the sublattice. The last term in Eq. (8) shows that whenever the intracell dimer separation b is nonzero, the electric field dynamically breaks the chiral symmetry of the system given by the operator σ_z. It is well known that in the static regime, without chiral symmetry, the SSH chain is in a topologically trivial phase.

The Schrödinger equation for the time-dependent Hamiltonian (7) is

$$i\hbar\partial_t|\Psi(t)\rangle = H(t)|\Psi(t)\rangle, \tag{9}$$

and its solution can be written as a linear combination of the eigenstates of H_S,

$$|\Psi(t)\rangle = \sum_{\ell=1}^{N}\sum_{s=\pm}c_{\ell,s}(t)|\ell\rangle|s\rangle, \tag{10}$$

where $|s\rangle$ is the eigenvector related to the sublattice space. To solve the dynamical evolution equation, we first perform a unitary transformation $|\Psi(t)\rangle = P(t)|\Phi(t)\rangle$ into the time-dependent Schrödinger equation, where $P(t)P^\dagger(t) = \mathbb{1}_\sigma\mathbb{1}_N$, with $\mathbb{1}_N$ being the N-dimensional identity operator. Therefore, we get the transformed Hamiltonian

$$\mathcal{H}(t) = P^\dagger(t)H(t)P(t) - i\hbar P^\dagger(t)\partial_t P(t). \tag{11}$$

Up to now, the result is valid for any general time-dependent problem. Now we choose

$$i\hbar\partial_t P(t) = V(t)P(t), \tag{12}$$

whose solution is given by

$$P(t) = e^{iB(t)\sigma_z/2}\sum_{\ell=1}^{N}p_\ell(t)|\ell\rangle\langle\ell|, \tag{13}$$

where $p_\ell(t) = \exp[-i(a/b)(\ell - N/2 - 1/2)B(t)]$ and $B(t) = (eb/\hbar)\int^t\mathcal{E}(t')dt'$. Since this unitary transformation also satisfies $[P(t), V(t)] = 0$, the transformed Hamiltonian then reads

$$\mathcal{H}(t) = P^\dagger(t)H_S P(t). \tag{14}$$

The effective time-dependent Hamiltonian is given as

$$\begin{aligned}\mathcal{H}(t) = {} & v\sum_{\ell=1}^{N}|\ell\rangle\langle\ell|(e^{-iB(t)}\sigma_+ + \text{H.c.}) \\ & + w\sum_{\ell=1}^{N-1}[p(t)|\ell+1\rangle\langle\ell|e^{-iB(t)}\sigma_+ + \text{H.c.}],\end{aligned} \tag{15}$$

where $p(t) = \exp[i(a/b)B(t)]$. For the effective electric field $\mathcal{E}(t) = \mathcal{E}_0\cos\Omega t$, we get

$$\begin{aligned}\mathcal{H}(t) = {} & v\sum_{\ell=1}^{N}|\ell\rangle\langle\ell|(e^{-irg\sin\Omega t}\sigma_+ + \text{H.c.}) \\ & + w\sum_{\ell=1}^{N-1}[|\ell+1\rangle\langle\ell|e^{i(1-r)g\sin\Omega t}\sigma_+ + \text{H.c.}],\end{aligned} \tag{16}$$

where $g = ea\mathcal{E}_0/\hbar\Omega$ is the effective light-matter coupling and $r = b/a$ is the distance ratio. The unitary transformation employed is a Kramers-Henneberger transformation [37]. This approach shows some advantages with respect to other perturbation schemes, such as the Brillouin-Wigner (BW) and the Floquet Magnus expansion (FME) methods. The BW perturbation method solves the energy spectrum in a self-consistent fashion and relies on the interaction to be much

smaller than the energy separation of the unperturbed levels [50–52]. Similarly, the FME involves the convergence of a series expansion expressed in terms of time integrals of the perturbation and its nth-order commutators at different times [53,54]. For a sinusoidal modulation, the maximum value of the effective light-matter coupling strength $g = \pi/4$ is required for the FME to converge. Therefore, neither the BW nor the FME is suitable for dealing with the strong light-matter coupling regime described in this work, for which we are considering g larger than $\pi/4$. Conversely, the Kramers-Henneberger transformation leads to an effective description of the light-matter interaction, in which the coupling parameter is encoded in Bessel functions, that are always restricted to the interval (0,1), for any value of the effective light-matter coupling strength. This enables us to study the strong light-matter coupling regime without including a large number of sidebands. In fact, applying the standard Floquet theory directly to the driven SSH system, would require the inclusion of 150 sidebands for the quasienergy spectrum to converge [17]. By contrast, the Kramers-Henneberger yields the quasienergy spectrum in terms of the zero order renormalized sideband contribution. Furthermore, this approach is applicable to amplitude modulated pulses without resorting to the $t - t'$ formalism.

The Floquet theorem states that the solution of a time-periodic Hamiltonian can be expressed as a linear combination of functions sharing the same periodicity [55,56]

$$|\Psi(t)\rangle = \sum_{\alpha} f_{\alpha}\phi_{\alpha}^{F}(t). \tag{17}$$

Here, $\phi_{\alpha}^{F}(t) = e^{-iE_{\alpha}t/\hbar}u_{\alpha}(t)$ is called the Floquet function and can be expressed as a periodic function $u_{\alpha}(t)$ modulated by a nonperiodic part depending on an exponent E_{α}. Since $u_{\alpha}(t)$ is periodic, we can expand it in its Fourier components

$$u_{\alpha}(t) = \sum_{m=-\infty}^{\infty} e^{im\Omega t}u_{\alpha,m}. \tag{18}$$

Substituting this into the definition of the Floquet function gives

$$\phi_{\alpha}^{F}(t) = e^{-i\xi_{\alpha,m}t/\hbar}u_{\alpha,m}, \tag{19}$$

where $\xi_{\alpha,m} = E_{\alpha} - m\hbar\Omega$ is called the quasienergy, stemming from the fact that, for a time-dependent Hamiltonian, energy is not a conserved quantity (for further discussion, see Ref. [57]). This decomposition can be used to find an equivalent formulation to the explicitly time-dependent Hamiltonian $\mathcal{H}(t)$ in terms of its Floquet-Fourier coefficients

$$H_{mm'} = \frac{1}{T}\int_{0}^{T}\mathcal{H}(t)e^{i(m-m')\Omega t}dt - m\hbar\Omega\delta_{mm'}\mathbb{1}_{2N}, \tag{20}$$

where $\mathbb{1}_{2N} = \mathbb{1}_{\sigma}\sum_{\ell=1}^{N}|\ell\rangle\langle\ell|$ is the $2N \times 2N$ identity matrix describing the dimer and lattice sites subspace for a chain with N dimers. The pulse period is $T = 2\pi/\Omega$. In practice, the Fourier series to build the Floquet-Fourier matrix is truncated for a maximum number of replicas $M_{\max}$ so that the spectrum, DOS, and other physical quantities of interest are not modified upon introducing additional Floquet replicas. Thus, the full Floquet-Fourier Hamiltonian can be written as

$$\mathcal{H}_{\mathrm{FF}} = \sum_{m,m'}^{M_{\max}} H_{mm'}|m\rangle\langle m'|, \tag{21}$$

where $|m\rangle$ is the space of the replicas.

Since the effective electric field is a monochromatic radiation field with constant amplitude, we can make use of the Jacobi-Anger expansion $\exp(iz\sin\Omega t) = \sum_{n=-\infty}^{\infty}J_n(z)\exp(in\Omega t)$ in terms of the Bessel functions of the first kind, to write the effective Hamiltonian (16) in the space of the Floquet replicas. Using the orthogonality relation $(1/T)\int_0^T e^{i(m-m')\Omega t}dt = \delta_{mm'}$ we can write the Floquet-Fourier Hamiltonian (20) as

$$\begin{aligned} H_{mm'} = &\sum_{\ell=1}^{N}|\ell\rangle\langle\ell|\{vJ_n(g')[(-1)^n\sigma_+ + \sigma_-] \\ &- m\hbar\Omega\mathbb{1}_{\sigma}\delta_{mm'}\} + wJ_n(g'') \\ &\times\sum_{\ell=1}^{N-1}[(-1)^n|\ell+1\rangle\langle\ell|\sigma_+ + |\ell\rangle\langle\ell+1|\sigma_-], \end{aligned} \tag{22}$$

where $n = m' - m$, $g' = rg$, $g'' = (1-r)g$, and we have used the parity property of the Bessel functions $J_m(-z) = (-1)^m J_m(z)$. For large frequencies, i.e., when $w, v \ll \hbar\Omega$, one can approximate the Floquet-Fourier Hamiltonian as $\mathcal{H}_{\mathrm{FF}} \approx H_{00}$ with

$$\begin{aligned} H_{00} = &vJ_0(g')\sum_{\ell=1}^{N}|\ell\rangle\langle\ell|\sigma_x + wJ_0(g'') \\ &\times\sum_{\ell=1}^{N-1}(|\ell+1\rangle\langle\ell|\sigma_+ + |\ell\rangle\langle\ell+1|\sigma_-). \end{aligned} \tag{23}$$

From Eq. (23) we can see that the intracell dimer separation b effectively adds a modulation of the intracell hopping parameter v. Since Bessel functions are oscillatory bounded by $\max\{J_m(x)\} \leqslant 1$, when $b = 0$, only the intercell hopping w is renormalized. Here, the topological state disappears when $wJ_0(g) < v$ while the trivial state remains unchanged. In contrast, when $b \neq 0$ the modulation extends to intracell hopping as well, allowing for regions in g space where $vJ_0(g') < wJ_0(g'')$, thus allowing the emergence of a topological phase. Therefore, Eq. (23) highlights that although the intracell dimer separation parameter b dynamically controls the breaking of chiral symmetry, the resulting effective Floquet Hamiltonian preserves this symmetry. Moreover, b simultaneously tunes the intercell to intracell hopping ratio, thereby governing the emergence of topological phase transitions.

For the numerical discussion, we have considered w as our unit of energy. Therefore, the topological state is characterized by $0 \leqslant v < 1$. For a better comparison with the results reported in Ref. [27], we have obtained the spectra and eigenstates of a $N = 20$ SSH chain when driven by a high-frequency electric field (i.e., $\hbar\Omega = 10w$) in terms of the effective light-matter interaction strength g.

In addition to the topological characterization, in the following we discuss the time-averaged density of states (DOS), which provides information on the energy level occupation,

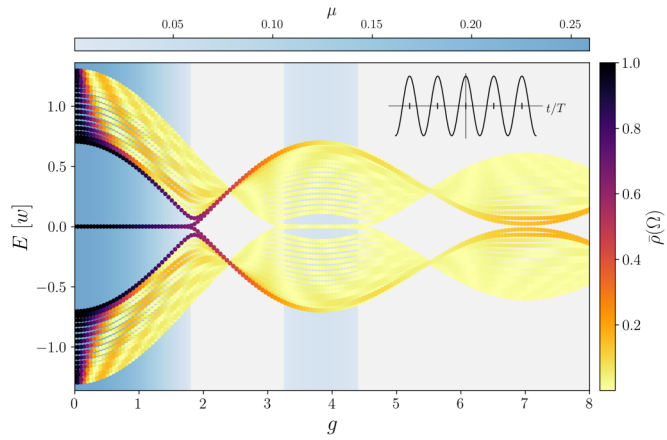

FIG. 2. Quasienergy spectrum within the off-resonant regime $\hbar\Omega/w = 10$, for the static topological phase $v/w = 0.3$ and $b = 0$. The color scale on the right represents the time-averaged DOS $\bar{\rho}$ associated with each quasienergy state in the FBZ. The inset shows the time-dependent profile of the applied electric field, and the ticks in its x axis represent the integrating regions of Eq. (20). $\bar{\rho}$ is obtained with $M = 20$ replicas and the shaded blue area gives the value of μ, as defined in Eq. (5), related to the signature of the spectral localizer (3).

as discussed below. In time-periodic systems described within the Floquet formalism, this quantity is usually defined as [11,58–60]

$$\bar{\rho}(\Omega) = \sum_{\alpha,m} |u_{\alpha,m}|^2 \delta(E_{\alpha,m} + m\hbar\omega - \hbar\Omega), \tag{24}$$

such that $\int \bar{\rho}(\Omega) d\Omega = 1$ and it can be interpreted as an occupation of the Floquet replicas. In our case, since nonperiodic pulses are also considered, we define it through the average over one period as

$$\bar{\rho}(\Omega) = \sum_{\alpha,m} \frac{1}{T} \int_0^T ||P(t)u_{\alpha,m}||^2 \delta(E_{\alpha,m} + m\hbar\omega - \hbar\Omega) dt. \tag{25}$$

In this way, we can spot when the gap opens or closes, and also quantify the value of the time-averaged DOS of the edge states. The quasienergy spectra can be obtained directly from Eq. (11) using the unitary transformation, without the need for replicas to ensure convergence. On the other hand, obtaining the time-averaged DOS, $\bar{\rho}$, requires $M = 20$ replicas to converge.

Figure 2 confirms the predicted behavior in which the trivial and nontrivial topological states change with increasing g, finding an emergent topological phase for $3.2 < g < 4.5$. Notice that, in this topological region, the zero-energy states exhibit an almost zero time-averaged DOS for the replica in the Floquet Brillouin zone (FBZ), which is the range of quasienergies represented in the figure. The DOS is displaced to Floquet replicas at higher energies, conserving the unitarity of the integrated spectral density $\int d\Omega \bar{\rho}(\Omega) = 1$. Furthermore, the DOS exhibits oscillatory behavior as g increases, with an oscillation frequency that increases with energy. The structure of the unitary transformation used suggests that these oscillations can be traced back to the modulation of the wave function expressed through the Bessel functions, which naturally arise from the expansion of the time-periodic driving field.

The next step is to confirm that, using the driving protocol, the time-averaged DOS of the FBZ can be controlled when a topologically nontrivial phase is induced via the driving starting from a static trivial phase [see Figs. 3(a) and 3(b)]. In Fig. 3(a) the evolution of the quasienegies as a function of g are calculated for an SSH chain with $b < 0.5a$. In this case, the topological phase ($g > 4.9$) shows zero-energy topological states with almost zero DOS. On the other hand, a system with $b > 0.5a$ [Fig. 3(b)] shows zero-energy states with a significant DOS and for lower values of g. This different behavior in the DOS of the induced topological state is due to the modulation rates of the hopping energies [see (16)]. In the nondriven SSH chain, the bulk spectrum is invariant under the exchange of $w \to v$ since the bulk dispersion is given by $E^2(k) = v^2 + w^2 + 2vw\cos k$.

However, in the finite nondriven chain, the topological phases are indeed characterized by the ratio of v/w such that edge states are present only if $|v/w| < 1$, i.e., the finite system has different phases under $w \to v$. Similarly, in the driven case, the bulk spectra is found to be equivalent between Figs. 3(a) and 3(b). However, the driven finite system exhibits different topological states when the two panels are compared.

The origin of this behavior lies in the parameter b. When $b/a < 0.5$, the effective hopping amplitude that vanishes in that electric field is the one proportional to w, while for $b/a > 0.5$, it is the amplitude proportional to v that becomes zero. Furthermore, as shown in Eq. (23), when b/a approaches 1, the condition $v < w$ is satisfied at lower values of g, which means that the system enters the topological phase for smaller amplitudes of the driving field. This is most relevant since the electric field amplitude is scaled by small quantities as the lattice parameter $a \sim 1$ nm and we are using high-frequency lasers. As a result, the actual electric field amplitude corresponds to $g \times 10^9$ V/m making it crucial to minimize g to keep the required field strength experimentally feasible. To conclude this section, it is worth stressing that while the intracell dimer separation instantaneously breaks the chiral symmetry when the ac electric field is applied, we have shown that there are some amplitudes at which a nontrivial topological phase exists and its associated edge states have a significant time-averaged DOS.

IV. DRIVING BY ELECTRIC FIELD WITH MODULATED AMPLITUDE

We extend now the analysis to amplitude modulated driving protocols, in which the amplitude of the driving field varies over time. To establish a connection to practical realizations, we focus on two relevant experimental scenarios: a Gaussian pulse, and a periodic envelope laser pulse. One strategy to tackle these problems is to employ the $t - t'$ formalism [28,33–36], which introduces two separate timescales for the envelope function and the faster oscillation. However, this method cannot be applied when the amplitude modulation is faster than the driving frequency, since it assumes adiabatic driving conditions. In this work, we use the unitary transformation (13), to overcome the limitations of the $t - t'$

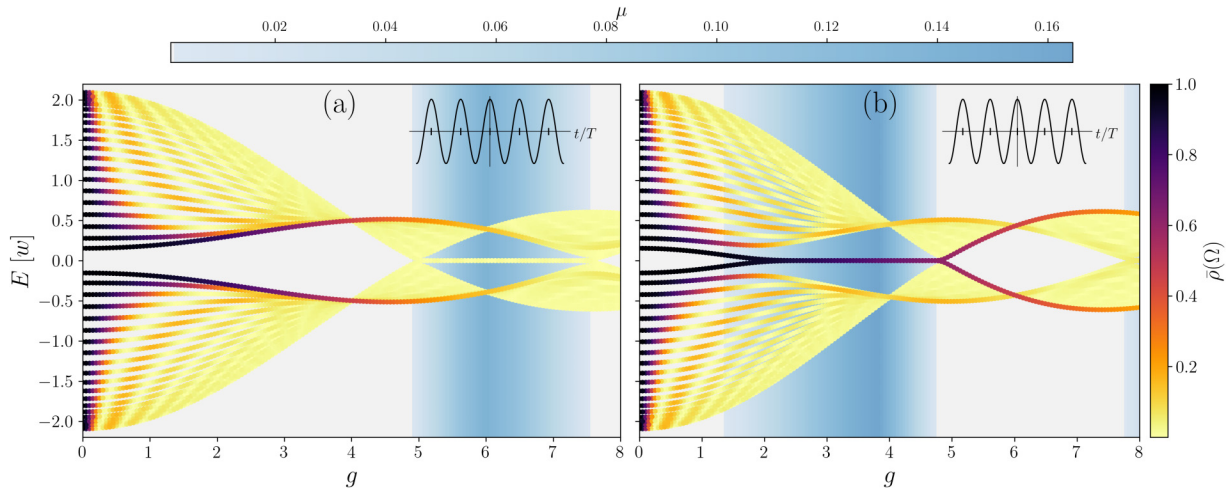

FIG. 3. Quasienergy spectra within the off-resonant regime $\hbar\Omega/w = 10$, for the static trivial phase $v/w = 1.1$ with (a) $b = 0.4a$ and (b) $b = 0.6a$ dimer separation. The other parameters and the color scales for the time-averaged DOS $\bar{\rho}$ and the spectral localizer μ are as in Fig. 2.

formalism and to propose an exact solution to the problem. In this section, we particularize the general expression (15) for the aforementioned driving protocols.

First, we define the function $F(t) = \Omega\,\mathcal{E}_0 f(t)\xi(t)$ where $f(t)$ is the envelope function of the periodic driving $\xi(t)$ with frequency Ω. Thus, the Hamiltonian (14) can be written as

$$\mathcal{H}(t) = v\sum_{\ell=1}^{N}|\ell\rangle\langle\ell|\left[\exp\left(-ig'\int F(t)dt\right)\sigma_+ + \text{H.c.}\right] + w\sum_{\ell=1}^{N}\left[|\ell+1\rangle\langle\ell|\exp\left(ig''\int F(t)dt\right)\sigma_+ + \text{H.c.}\right], \tag{26}$$

where g' and g'' are the same as defined after Eq. (22). Typically, the envelope function will not be periodic or it will have a different period to the driving. For this reason, the hopping modifiers cannot be easily decomposed into a discrete Floquet basis as it was in the static scenario, because they are now time dependent. To address this problem, we decompose the coefficients as $a_n = \int_0^T a_n(t)dt$, there T is the time period of the driving $T = 2\pi/\Omega$ (or Ω_- in the periodic envelope laser pulse discussed in the following).

A. Gaussian pulse

One of the most common pulse shapes used in driving experiments and measurements is the Gaussian envelope. Consequently, it is natural to investigate how the system behaves when the driving field is modulated by a Gaussian envelope function. We describe it as

$$\mathcal{E}(t) = \mathcal{E}_0 e^{-(t\Gamma)^2}\cos\Omega t, \tag{27}$$

with $1/\Gamma$ being proportional to the width of the pulse. Introducing dimensionless variables $\tau = \Omega t$, $c = \Omega/\Gamma$, we get for the modulation factor

$$\int F(t)dt = \frac{\sqrt{\pi}ce^{-c^2/4}}{2}\text{Re}\left[\text{erf}\left(\frac{\tau}{c} + \frac{ic}{2}\right)\right], \tag{28}$$

with the error function defined as [61]

$$\text{erf}(z) = \frac{2}{\sqrt{\pi}}\int_0^z e^{-\xi^2}d\xi, \tag{29}$$

where z is an arbitrary complex variable. As expected, in the limit $c \to \infty$, that is, $\Gamma \to 0$, we recover the former results for the constant-amplitude driving field.

The next step is substituting Eq. (28) into Eq. (26) and using the definition of the Floquet-Fourier Hamiltonian (20) to find the quasienergy spectrum and DOS. From Fig. 4 we see that the effect of the Gaussian pulse is to lift the bulk degeneracy at the points around $g = 4$ and $g = 6.5$ where one of the hopping parameters became zero. This lifting results in a spread of quasienergy levels, keeping the lowest-energy states with higher time-averaged DOS and thereby facilitating the occupation of subsequent topological states. However, we also observe that as the pulse duration decreases, as shown in Fig. 4 (b), where $\Gamma = 2\ \text{s}^{-1}$, the spectra extend toward higher values of g. In other words, the onset of the topological state is shifted to larger effective electric field strengths. This behavior is undesirable for practical experimental implementations as it would require higher irradiation power, potentially leading to sample damage.

B. Periodic envelope laser pulse

We now consider the driving-field configuration,

$$\mathcal{E}(t) = \mathcal{E}_0 f(t)\cos\Omega t, \tag{30}$$

where $\mathcal{E}_0$ is the maximum field amplitude, $\hbar\Omega \gg w, v$, and $f(t + T_2) = f(t)$, where $\omega = 2\pi/T_2$ is the frequency of the periodically varying amplitude, which does not need to be commensurate with the driving frequency. For instance, in the case $f(t) = \cos\omega t$ we get

$$\mathcal{E}(t) = \mathcal{E}_0\cos(\Omega t)\cos(\omega t), \tag{31}$$

which corresponds to a superposition of two laser pulses of equal amplitude producing a beating pattern of frequency $\Omega_- = \Omega - \omega$ and oscillatory frequency $\Omega_+ = \Omega + \omega$. Then,

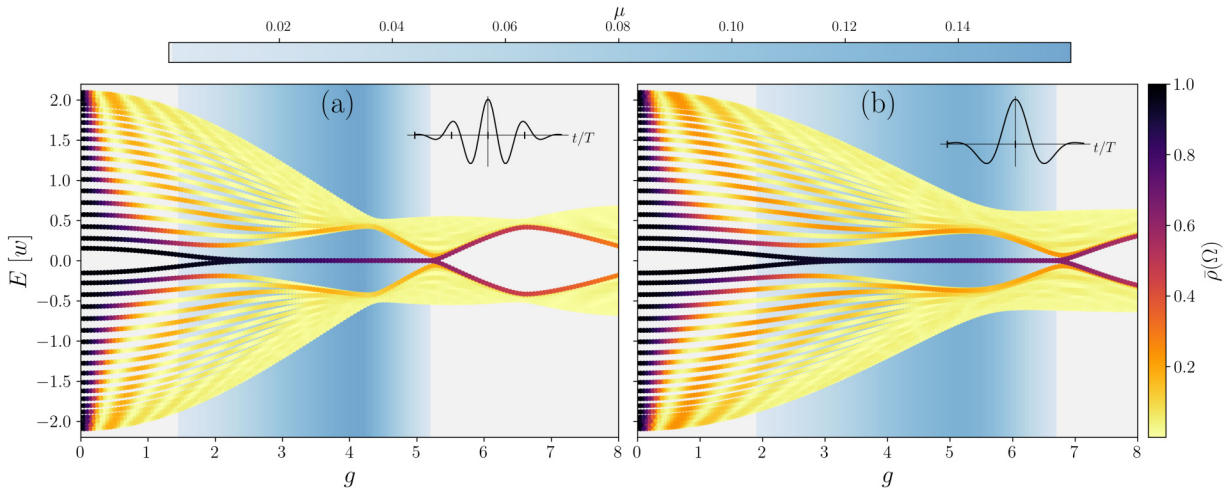

FIG. 4. Quasienergy spectrum within the off-resonant regime for the static trivial phase $v/w = 1.1$ with intracell dimer separation $b/a = 0.6$ for a Gaussian pulse with (a) $\Gamma = 1\ \mathrm{s}^{-1}$ and (b) $\Gamma = 2\ \mathrm{s}^{-1}$. The color scales represent the time-averaged DOS $\bar{\rho}$ and the spectral localizer μ as described in the caption of Fig. 2. The frequency of the electric field has been set to $\hbar\Omega/w = 10$. The inset shows the time-dependent profile of the applied electric field, and the ticks in its x axis represent the integrating regions of Eq. (20).

the effective electric field can be written as

$$\mathcal{E}(t) = \frac{\mathcal{E}_0}{2}(\cos\Omega_+ t + \cos\Omega_- t). \tag{32}$$

So we can understand this modulation as the use of two different harmonic waves for the driving, one for driving (fast one) and the other for probe. The effective modulation of the hopping now reads

$$\int F(t)dt = \frac{\Omega}{2\Omega_+}\sin\Omega_+ t + \frac{\Omega}{2\Omega_-}\sin\Omega_- t, \tag{33}$$

and in the limit when $\omega \approx 0$ we have $\Omega_+ \approx \Omega_- \approx \Omega$ so that we recover the situation previously discussed. Here, we can use the Jacobi-Anger expansion to write the effective intracell hopping modulation $p_v(t)$ as

$$p_v(t) = \sum_{m_1=-\infty}^{\infty} J_{m_1}\left(-g'\frac{\Omega}{\Omega_+}\right)e^{im_1\Omega_+ t} \times \sum_{m_2=-\infty}^{\infty} J_{m_2}\left(-g'\frac{\Omega}{\Omega_-}\right)e^{im_2\Omega_- t}, \tag{34}$$

with the effective modulation of the intercell hopping $p_w(t)$ being the same with the change $g' \to g''$. As driving is now composed of two distinct frequencies, the original driving frequency Ω is no longer representative of the system's periodicity [see Eq. (34)]. Therefore, in Eq. (20), we replace Ω by Ω_-, the lower of the two driving frequencies. This choice is particularly relevant since selecting the lower frequency al-

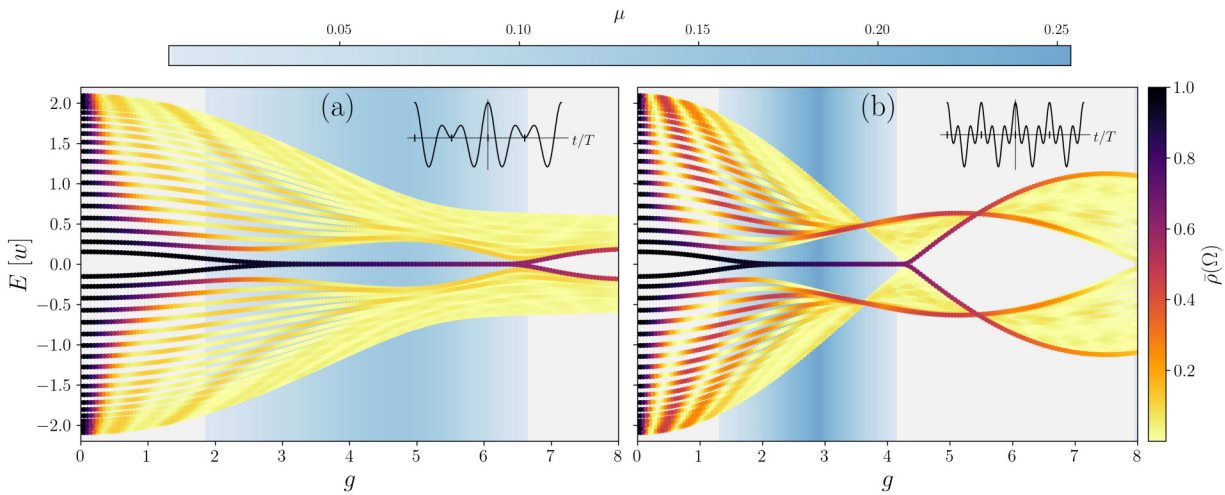

FIG. 5. Quasienergy spectrum within the off-resonant regime for the static trivial phase $v/w = 1.1$ with intracell dimer separation $b/a = 0.6$ for a periodic envelope laser pulse with (a) $\hbar\omega/w = 2$ and (b) $\hbar\omega/w = 5$. The color scales represent the time-averaged DOS $\bar{\rho}$ and the spectral localizer μ as described in the caption of Fig. 2. The frequency of the electric field has been set to $\hbar\Omega/w = 10$. The inset shows the time-dependent profile of the applied electric field.

lows for a denser sampling of the time-dependent quasienergy spectrum, thereby capturing features that would be missed with a larger replica spacing such as that induced by Ω_+.

The quasienergy spectra and the time-averaged DOS are sketched in Fig. 5. When the envelope frequency ω is small, the behavior resembles that of the Gaussian pulse: The degeneracies around specific values of g are lifted, and the spectrum is shifted to higher-field amplitudes. However, as ω increases and approaches the driving frequency Ω, new degeneracies reappear in the spectrum and the transition to topological states is achieved at lower values of the effective light-matter coupling strength g. This indicates a nontrivial interplay between the two timescales, which could be exploited to obtain these unconventional Floquet topological phases in the presence of dynamical chiral symmetry-breaking interactions. Notably, these phases can emerge under less intense effective radiation fields compared to those required in the constant-amplitude driving protocol.

V. CONCLUSIONS

In this work, we have analyzed the effect of an ac electric field applied to an SSH chain in the tuning of its topological phase. To this end, we employed a Kramers-Henneberger-like transformation, which effectively maps the contributions from all Floquet replicas onto the first one. We show that the system can be driven between the trivial and topological phases by varying the amplitude of the applied ac electric field. Furthermore, we demonstrated that topological phases can persist even when the intracell dimer separation is nonzero and the chiral symmetry is explicitly broken due to time-periodic perturbation. To induce topological phases under realistic field strengths, larger intracell dimer separations are shown to be advantageous. It is worth noting that not all the topological states have a significant time-averaged DOS at zero energy and different DOS configurations can be tuned with the external driving. Although nonperiodic driving protocols have traditionally been analyzed using perturbation-based methods or the Floquet $t - t'$ formalism, our Kramers-Henneberger-like transformation enables the treatment of arbitrary nonperiodic dynamical effects without imposing constraints on the rate of change and amplitudes of the perturbation. We have also shown that Gaussian pulses shift the quasienergy spectrum to higher electric field amplitudes and lift degeneracies in the trivial energies, thereby enabling higher-field topological states to show a significant DOS. In contrast, periodic envelope modulations can shift the spectrum to lower-field amplitudes when the envelope frequency approaches the driving frequency ($\omega \sim \Omega$). Therefore, our results suggest that the optimal configuration for experimental realization involves an SSH chain with large intracell dimer separation driven by a high-frequency electric field modulated with a fast periodic envelope. However, it is important to highlight that these conditions for finite sideband DOS of the zero-energy topological states could be relevant for spectroscopy observations through time-resolved and angle-resolved photoemission spectroscopy as reported in Refs. [31,32,62,63]. On the other hand, there could be other configurations (e.g., the measurement of edge states through a transport setup) where it might be desirable to have an unpopulated non trivial energy state, as they could be detected via conductance peaks occurring at different values of the bias gate voltage.

ACKNOWLEDGMENTS

The authors thank G. Platero and R. A. Molina for helpful discussions. Work in Madrid has been supported by the Comunidad de Madrid (Recovery, Transformation and Resilience Plan) and NextGenerationEU from the European Union (Grant No. MAD2D-CM-UCM5) and the Agencia Estatal de Investigación (Grant No. PID2022-136285NB-C31). R.P.A.L. acknowledges support from BG23/00151 action (MCINU, Spain). P.O. acknowledges support from DGIIE USM PI-LIR-24-10, FONDECYT under Grants No. 122070 and No. 1230933.

DATA AVAILABILITY

The data that support the findings of this article are not publicly available. The data are available from the authors upon reasonable request.

[1] K. v. Klitzing, G. Dorda, and M. Pepper, New method for high-accuracy determination of the fine-structure constant based on quantized Hall resistance, Phys. Rev. Lett. **45**, 494 (1980).

[2] F. D. M. Haldane, Model for a quantum Hall effect without Landau levels: Condensed-matter realization of the "parity anomaly", Phys. Rev. Lett. **61**, 2015 (1988).

[3] C. L. Kane and E. J. Mele, Quantum spin Hall effect in graphene, Phys. Rev. Lett. **95**, 226801 (2005).

[4] B. A. Bernevig, T. L. Hughes, and S.-C. Zhang, Quantum spin Hall effect and topological phase transition in HgTe quantum wells, Science **314**, 1757 (2006).

[5] M. König, S. Wiedmann, C. Brüne, A. Roth, H. Buhmann, L. W. Molenkamp, X.-L. Qi, and S.-C. Zhang, Quantum spin Hall insulator state in HgTe quantum wells, Science **318**, 766 (2007).

[6] M. Z. Hasan and C. L. Kane, Colloquium: Topological insulators, Rev. Mod. Phys. **82**, 3045 (2010).

[7] A. Alexandradinata, C. Fang, M. J. Gilbert, and B. A. Bernevig, Spin-orbit-free topological insulators without time-reversal symmetry, Phys. Rev. Lett. **113**, 116403 (2014).

[8] T. Oka and H. Aoki, Photovoltaic Hall effect in graphene, Phys. Rev. B **79**, 081406(R) (2009).

[9] B. Dóra, K. Ziegler, P. Thalmeier, and M. Nakamura, Rabi oscillations in Landau-quantized graphene, Phys. Rev. Lett. **102**, 036803 (2009).

[10] N. H. Lindner, G. Refael, and V. Galitski, Floquet topological insulator in semiconductor quantum wells, Nat. Phys. **7**, 490 (2011).

[11] G. Usaj, P. M. Perez-Piskunow, L. E. F. Foa Torres, and C. A. Balseiro, Irradiated graphene as a tunable Floquet topological insulator, Phys. Rev. B **90**, 115423 (2014).
[12] A. G. Grushin, A. Gómez-León, and T. Neupert, Floquet fractional Chern insulators, Phys. Rev. Lett. **112**, 156801 (2014).
[13] P. Titum, N. H. Lindner, and G. Refael, Disorder-induced transitions in resonantly driven Floquet topological insulators, Phys. Rev. B **96**, 054207 (2017).
[14] I. Esin, M. S. Rudner, G. Refael, and N. H. Lindner, Quantized transport and steady states of Floquet topological insulators, Phys. Rev. B **97**, 245401 (2018).
[15] Y. Peng and G. Refael, Floquet second-order topological insulators from nonsymmorphic space-time symmetries, Phys. Rev. Lett. **123**, 016806 (2019).
[16] X.-L. Lü and H. Xie, Topological phases and pumps in the Su-Schrieffer-Heeger model periodically modulated in time, J. Phys.: Condens. Matter **31**, 495401 (2019).
[17] A. Gómez-León, Anomalous Floquet phases. A resonance phenomena, Quantum **8**, 1522 (2024).
[18] P. Molignini, W. Chen, and R. Chitra, Universal quantum criticality in static and Floquet-Majorana chains, Phys. Rev. B **98**, 125129 (2018).
[19] P. Molignini, W. Chen, and R. Chitra, Generating quantum multicriticality in topological insulators by periodic driving, Phys. Rev. B **101**, 165106 (2020).
[20] P. Molignini, J. C. Budich, and B. Trauzettel, Unifying topological phase transitions in non-interacting, interacting, and periodically driven systems, Europhys. Lett. **128**, 36001 (2020).
[21] P. Molignini, Edge mode manipulation through commensurate multifrequency driving, Phys. Rev. B **102**, 235143 (2020).
[22] A. Kitaev, Periodic table for topological insulators and superconductors, AIP Conf. Proc. **1134**, 22 (2009).
[23] A. P. Schnyder, S. Ryu, A. Furusaki, and A. W. W. Ludwig, Classification of topological insulators and superconductors in three spatial dimensions, Phys. Rev. B **78**, 195125 (2008).
[24] C.-K. Chiu, J. C. Y. Teo, A. P. Schnyder, and S. Ryu, Classification of topological quantum matter with symmetries, Rev. Mod. Phys. **88**, 035005 (2016).
[25] C.-K. Chiu, H. Yao, and S. Ryu, Classification of topological insulators and superconductors in the presence of reflection symmetry, Phys. Rev. B **88**, 075142 (2013).
[26] J. Langbehn, Y. Peng, L. Trifunovic, F. von Oppen, and P. W. Brouwer, Reflection-symmetric second-order topological insulators and superconductors, Phys. Rev. Lett. **119**, 246401 (2017).
[27] A. Gómez-León and G. Platero, Floquet-Bloch theory and topology in periodically driven lattices, Phys. Rev. Lett. **110**, 200403 (2013).
[28] Y. Baba, V. Junk, W. Hogger, F. Domínguez-Adame, R. A. Molina, and K. Richter, Radiation-induced dynamical formation of Floquet-Bloch bands in Dirac Hamiltonians, New J. Phys. **27**, 043015 (2025).
[29] S. Ito, M. Schüler, M. Meierhofer, S. Schlauderer, J. Freudenstein, J. Reimann, D. Afanasiev, K. A. Kokh, O. E. Tereshchenko, J. Güdde, M. A. Sentef, U. Höfer, and R. Huber, Build-up and dephasing of Floquet-Bloch bands on subcycle timescales, Nature (London) **616**, 696 (2023).
[30] J. W. McIver, B. Schulte, F.-U. Stein, T. Matsuyama, G. Jotzu, G. Meier, and A. Cavalleri, Light-induced anomalous Hall effect in graphene, Nat. Phys. **16**, 38 (2020).
[31] M. Merboldt, M. Schüler, D. Schmitt, J. P. Bange, W. Bennecke, K. Gadge, K. Pierz, H. W. Schumacher, D. Momeni, D. Steil, S. R. Manmana, M. A. Sentef, M. Reutzel, and S. Mathias, Observation of Floquet states in graphene, Nat. Phys. **21**, 1093 (2025).
[32] D. Choi, M. Mogi, U. De Giovannini, D. Azoury, B. Lv, Y. Su, H. Hübener, A. Rubio, and N. Gedik, Observation of Floquet–Bloch states in monolayer graphene, Nat. Phys. **21**, 1100 (2025).
[33] K. Drese and M. Holthaus, Floquet theory for short laser pulses, Eur. Phys. J. D **5**, 119 (1999).
[34] M. Holthaus, Floquet engineering with quasienergy bands of periodically driven optical lattices, Eur. Phys. J. B **49**, 013001 (2015).
[35] T. N. Ikeda, S. Tanaka, and Y. Kayanuma, Floquet-Landau-Zener interferometry: Usefulness of the Floquet theory in pulse-laser-driven systems, Phys. Rev. Res. **4**, 033075 (2022).
[36] A. S. Gómez, Y. Baba, F. Domínguez-Adame, and R. A. Molina, Time-dependent dichroism and transient valley polarization in monolayer transition metal dichalcogenides under finite-pulse radiation, J. Phys.: Mater. **8**, 035005 (2025).
[37] W. C. Henneberger, Perturbation method for atoms in intense light beams, Phys. Rev. Lett. **21**, 838 (1968).
[38] W. P. Su, J. R. Schrieffer, and A. J. Heeger, Solitons in polyacetylene, Phys. Rev. Lett. **42**, 1698 (1979).
[39] M. Atala, M. Aidelsburger, J. T. Barreiro, D. Abanin, T. Kitagawa, E. Demler, and I. Bloch, Direct measurement of the Zak phase in topological Bloch bands, Nat. Phys. **9**, 795 (2013).
[40] C. Li, S. Lin, G. Zhang, and Z. Song, Topological nodal points in two coupled Su-Schrieffer-Heeger chains, Phys. Rev. B **96**, 125418 (2017).
[41] V. Dal Lago, M. Atala, and L. E. F. Foa Torres, Floquet topological transitions in a driven one-dimensional topological insulator, Phys. Rev. A **92**, 023624 (2015).
[42] C. Borja, E. D. Gutiérrez, and A. López, Emergence of Floquet edge states in the coupled Su-Schrieffer-Heeger model, J. Phys.: Condens. Matter **34**, 205701 (2022).
[43] D. J. Thouless, M. Kohmoto, M. P. Nightingale, and M. den Nijs, Quantized Hall conductance in a two-dimensional periodic potential, Phys. Rev. Lett. **49**, 405 (1982).
[44] S. Ryu and Y. Hatsugai, Topological origin of zero-energy edge states in particle-hole symmetric systems, Phys. Rev. Lett. **89**, 077002 (2002).
[45] R. Bianco and R. Resta, Mapping topological order in coordinate space, Phys. Rev. B **84**, 241106(R) (2011).
[46] I. Mondragon-Shem, T. L. Hughes, J. Song, and E. Prodan, Topological criticality in the chiral-symmetric AIII class at strong disorder, Phys. Rev. Lett. **113**, 046802 (2014).
[47] T. A. Loring and H. Schulz-Baldes, Spectral flow argument localizing an odd index pairing, Can. Math. Bull. **62**, 373 (2019).
[48] A. Cerjan and T. A. Loring, Classifying photonic topology using the spectral localizer and numerical k-theory, APL Photonics **9**, 111102 (2024).
[49] A. K. Ghosh, R. Arouca, and A. M. Black-Schaffer, Local and energy-resolved topological invariants for Floquet systems, Phys. Rev. B **110**, 245306 (2024).
[50] J. E. Lennard-Jones, Perturbation problems in quantum mechanics, Proc. R. Soc. A **129**, 598 (1930).
[51] L. Brillouin, Les problèmes de perturbations et les champs self-consistents, J. Phys. Radium **3**, 373 (1932).

[52] E. P. Wigner, On a Modification of the Rayleigh-Schrödinger Perturbation Theory, in *Part I: Physical Chemistry. Part II: Solid State Physics*, The Collected Works of Eugene Paul Wigner, vol. A/4, edited by A. S. Wightman (Springer, Berlin, Heidelberg, 1997).

[53] W. Magnus, On the exponential solution of differential equations for a linear operator, Commun. Pure Appl. Math. **7**, 649 (1954).

[54] S. Blanes, F. Casas, J. A. Oteo, and J. Ros, The Magnus expansion and some of its application, Phys. Rep. **470**, 151 (2009).

[55] J. H. Shirley, Solution of the Schrödinger equation with a Hamiltonian periodic in time, Phys. Rev. **138**, B979 (1965).

[56] M. Grifoni and P. Hänggi, Driven quantum tunneling, Phys. Rep. **304**, 229 (1998).

[57] U. D. Giovannini and H. Hübener, Floquet analysis of excitations in materials, J. Phys. Mater. **3**, 012001 (2020).

[58] G. S. Uhrig, M. H. Kalthoff, and J. K. Freericks, Positivity of the spectral densities of retarded Floquet Green functions, Phys. Rev. Lett. **122**, 130604 (2019).

[59] M. S. Rudner and N. H. Lindner, Band structure engineering and non-equilibrium dynamics in Floquet topological insulators, Nat. Rev. Phys. **2**, 229 (2020).

[60] M. S. Rudner and N. H. Lindner, The Floquet engineer's handbook, arXiv:2003.08252.

[61] E. T. Whittaker, G. N. Watson, and V. H. Moll, *A Course of Modern Analysis*, 5th ed. (Cambridge University Press, Cambridge, U.K., 2021).

[62] Y. H. Wang, H. Steinberg, P. Jarillo-Herrero, and N. Gedik, Observation of Floquet-Bloch states on the surface of a topological insulator, Science **342**, 453 (2013).

[63] F. Mahmood, C. K. Chan, Z. Alpichshev, D. Gardner, Y. Lee, P. A. Lee, and N. Gedik, Selective scattering between Floquet–Bloch and Volkov states in a topological insulator, Nat. Phys. **12**, 306 (2016).